Resonance Raman Spectroscopic Investigation of Directly Linked Zinc(II) Porphyrin Linear Arrays†

Dae Hong Jeong, Min-Chul Yoon, Sung Moon Jang, and Dongho Kim*

Center for Ultrafast Optical Characteristics Control and Department of Chemistry, Yonsei University, Seoul 120-749, Korea

Dae Won Cho

Department of Chemistry, Seonam University, Namwon 590-711, Korea

Naoya Yoshida, Naoki Aratani, and Atsuhiro Osuka*

Department of Chemistry, Graduate School of Science, Kyoto University, Kyoto 606-8502, Japan

Received: August 31, 2001; In Final Form: December 31, 2001

We have investigated the resonance Raman (RR) spectra of the directly linked porphyrin arrays in order to elucidate the relationship between excitonic interactions and molecular geometry depending on the number of pigments in the arrays. The RR spectra obtained by photoexcitation at the high-energy exciton Soret bands in the arrays are mainly composed of Raman modes localized on the constituent porphyrin monomers. In contrast, the RR spectra of the arrays with photoexcitation at the low-energy exciton split Soret bands reveal some characteristic Raman bands arising from strong excitonic interactions between the adjacent porphyrins in the arrays. Based on the RR measurements of the isotope labeled analogues and the normal-mode analysis of the dimer, it is suggested that the photoexcitation at the high-energy Soret band produces an electronically excited state largely localized within a monomer unit and that at the low-energy exciton split Soret band the excited state is in a way delocalized throughout the array. Normal mode calculation revealed that some of the RR bands of Z2 arise from vibrational splitting by dimeric interactions. Phonon-like behaviors were observed for some C_m-C_m stretching modes of the arrays, which is ascribed to enhanced polarizability induced by phenyl group movement. Collectively, our data from RR spectroscopic measurements as well as the normal-mode analysis provide a picture of the exciton coupling in relation to the molecular structure of the directly linked linear porphyrin arrays.

I. Introduction

Natural light-gathering arrays have been an ideal target in biomimetic design for the fabrication of molecular photonic devices.[1−9] As a result of continuing efforts to realize the mimicry of solar energy harvesting complexes, much improvement has been made in synthesizing and isolating a variety of covalently linked *multi*porphyrin arrays.[10−13] The recent success in elaborating various porphyrin architectures using several types of linkers via meso position attachment has brought up the issues on the *inter*chromophore electronic interactions, of which the extent is determined by the interconnection length and relative orientation between the adjacent porphyrin moieties. Recently, the direct meso−meso connection has been accomplished, leading to substantially strong dipole−dipole interactions between the adjacent porphyrin units to exhibit a large exciton coupling energy of approximately 4300 cm^{-1}.[14,15]

The meso−meso direct linkage of the porphyrin arrays affords interesting features. The unshifted and red-shifted Soret excitonic bands are both originated from the same Soret transitions but show totally different natures: the former has monomeric character but the latter dimeric character.[16] The RR enhancement for the two closely lying strong transitions are of interest especially with respect to the vibronic interaction between them. The distance between the adjacent porphyrin rings is very close (ca.. 1.4 Å) even though the center-to-center distance is ca. 8.35 Å. The average *inter*porphyrin geometry is kept orthogonal due to a large steric hindrance caused by the close proximity of the constituent porphyrin rings. These facts make it possible that the porphyrin arrays show unusually large excitonic splitting in the Soret transitions.[16] The decreased *inter*porphyrin distance and, consequently, the strong exciton interaction yield the prospects for the much sought-after *intra*dimer vibrational splitting in the resonance Raman spectra.[17,18] The basic frame of the dimer interaction was described theoretically by Fulton and Gourterman[19] and the rules for vibrational splitting were presented by Adar and Srivastava.[20] However, the dimer splitting could not be observed in μ-oxo and nitrido porphyrin dimers[17] and axially bridged porphyrin dimers via direct metal−metal bonds.[18]

With these facts in mind, we have sought to probe the RR spectra of the directly linked porphyrin arrays by photoexcitations at the two Soret excitonic bands. Then, we discuss the differences in the RR spectra caused by the different electronic nature between the two excitonic bands. Next, we look for evidence on the vibrational splitting induced by *intra*dimer excitonic coupling of the porphyrin units. The dimeric interaction is addressed in relation to the phonon-like behaviors of the longer arrays. For the above discussion, the normal-mode analysis is discussed based on the isotope RR experiments to assign the vibrational modes of the porphyrin arrays.

† Part of the special issue "Noboru Mataga Festschrift".

* To whom correspondence should be addressed. Fax: 82-2-2123-2434. Electric mail: dongho@yonsei.ac.kr.

10.1021/jp0132331 CCC: $22.00
Published on Web 02/07/2002

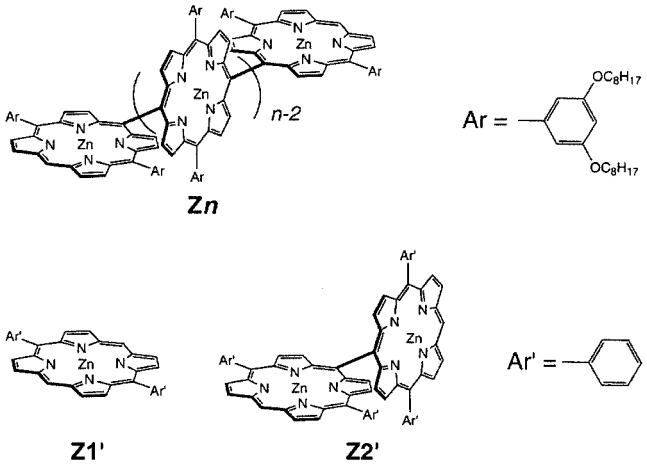

Figure 1. Molecular structures of the porphyrin arrays. *n* in Z*n* is the number of porphyrin units. Z1′ and Z2′ are the analogues of Z1 and Z2 with phenyl rings substituted as peripheral groups.

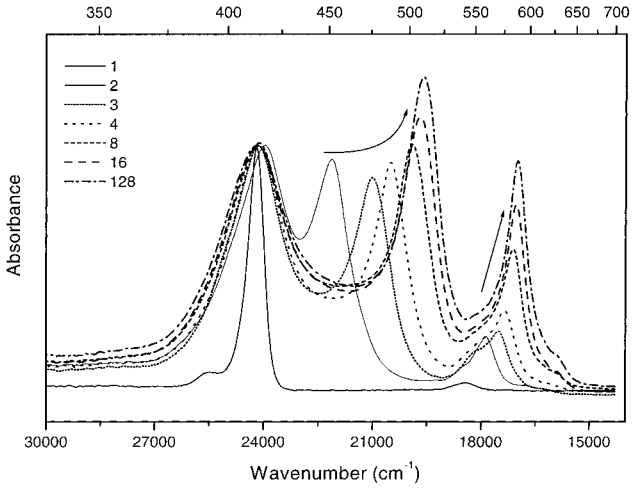

Figure 2. Series of ground-state absorption spectra of the porphyrin arrays in THF.

II. Experimental Section

Zn(II) 5,15-bis(3,5-dioctyloxyphenyl)porphyrin (Z1) (we denote the meso−meso-coupled Zn(II) porphyrin arrays as Z*n* where *n* represents the number of porphyrins), and its meso, meso-linked porphyrin arrays from dimer (Z2) to Z128 oligomer were synthesized through repetitive Ag^{I}-promoted meso−meso-coupling reactions.[14,15] The schematic diagram of the porphyrin arrays are shown in Figure 1. The analogous phenyl-substituted porphyrin monomer (Z1′) and dimer (Z2′) were also prepared (Figure 1c). Their isotope labeled analogues (^{13}C−Z1′ and ^{13}C−Z2′, respectively) in which ^{13}C is substituted at the 5,15 meso positions were synthesized. The recycling GPC−HPLC was used for product separation. MALDI-TOF mass and ^{1}H NMR spectra were employed for product characterization. The spectroscopic grade tetrahydrofuran (THF) was used as a solvent for all experiments. The absorption spectra were recorded by using a Varian Cary 3 spectrophotometer.

The ground-state RR spectra of the porphyrin arrays were obtained by photoexcitation using six lines (457.9, 476.5, 488.0, 496.5, 501.7, and 514.5 nm) from a continuous wave (cw) Ar ion laser (Coherent INNOVA 90).[21] These lines correspond to the low-energy exciton split Soret bands of the porphyrin arrays. Raman scattering signals were collected in 90° scattering geometry and detected by a 1-m double monochromator (ISA Jobin-Yvon U-1000) equipped with a thermoelectrically cooled photomultiplier tube (Hamamatsu R943−02). For excitation at the high-energy Soret bands of the porphyrin arrays at ca. 415 nm, 416 nm line was generated by the hydrogen Raman shifting of the third harmonics (355 nm) from a nanosecond Q-switched Nd:YAG laser. The Raman spectra were recorded by a single pass spectrometer (ISA Jobin-Yvon HR640) with a gated intensified charge-coupled device (ICCD, Princeton Instruments IRY700) detector and a pulse generator (Princeton Instruments FG100). For depolarization ratio measurement, a polarizer was placed between the collection lens and monochromator slit. A scrambler was placed after the polarizer in order to compensate the grating efficiency for light polarized horizontal and vertical to the incident polarization. The depolarization ratios for the Raman bands of CCl_4 were measured as a reference. A modified Pasteur pipet whose end has a tiny capillary tube attached was used as a Raman cell in order to make sample solution flow to minimize its consumption and photodecomposition by the cw laser excitation. Normal mode calculation was carried out using the semiempirical AM1 method for Z1′ and Z2′. The normal modes of Zn^{II}TPP also were calculated with the same method to correlate the current calculation with that in the references.

III. Results

Steady-State UV−Visible Absorption Spectra. The absorption spectra of the directly linked Zn(II)porphyrin linear arrays in THF are shown in Figure 2. As the number of porphyrin units increases in the arrays, the splitting of the Soret bands becomes more pronounced, exhibiting two well-separated Soret bands to the blue side of the relatively unperturbed Q-bands. The most striking feature is the systematic red shift of the lower-energy Soret band as the number of the porphyrin units in the arrays increases while the high-energy Soret band remains intact. The asymptotic feature of the separation of the two Soret bands is characteristic of excitonic interaction.[22] In addition, the orthogonal arrangement between the adjacent porphyrin units precludes effective π-electronic conjugation that is anticipated to shift the Q-bands to near-IR region as in the cases of butadiyne[23] or ethylene[11a,b,24] bridged porphyrin arrays.

These observations were successfully explained by using a molecular exciton model.[16] In the dimer case each porphyrin unit provides degenerate orthogonal transition dipoles of B_x and B_y (or B_z) for the Soret band, and consequently, four transition dipoles interact together resulting in two degenerate unshifted, one red-shifted, and one forbidden transitions (Figure 3). The unshifted band is due to the B_y and B_z components, which are orthogonal to each other as well as to the long axis of the porphyrin array. Since the interaction between the mutually orthogonal transitions is zero, the relevant transition appears at the same position as in the porphyrin monomer. The significantly broadened features of the unshifted bands of dimer and higher oligomers at ∼416 nm relative to the narrow Soret band of the monomer is presumably caused by a distribution of conformers that differ with respect to the torsional angle between the adjacent porphyrin planes.[25] The in-phase arrangement of two B_x components leads to electrostatic attraction, producing the red-shifted band. The out-of-phase arrangement of the two components causes repulsion, producing a blue-shifted band. However, this band is forbidden according to the selection rule by Kasha.[22] The same rules can be applied to the longer porphyrin arrays than Z2, which give rise to the same spectral features with larger splittings.

Overall, the electronic natures of the two Soret bands are totally different from each other, even though they originate from the same Soret bands. One of the most important

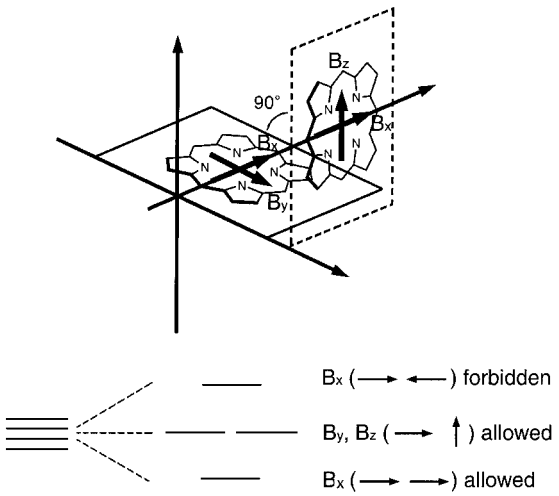

Figure 3. Schematic diagram of exciton splitting of the Soret bands in a porphyrin dimer.

implications is that the unperturbed high-energy Soret band is composed of the summation of transition dipoles of the constituent monomer units perpendicular to the long molecular axis, while the red-shifted exciton split Soret band has an overall transition dipole parallel to the long molecular axis of the porphyrin arrays. These unique features of the porphyrin arrays are likely to play a pivotal role in the RR scattering processes since the RR enhancement pattern is critically affected by the nature of the electronic states in resonance with the Raman excitation lines.

Resonance Raman Spectra of Porphyrin Arrays. The RR spectra of the porphyrin monomer and a series of porphyrin arrays with excitations at 435 and 416 nm, respectively, are depicted in Figure 4a, and those of the porphyrin monomer and arrays with excitations at their low-energy Soret bands are shown in Figures 4b and 5. The RR spectrum of Z1 with the Soret band excitation at 435 nm is similar to the previously reported one of Zn^{II}TPP (TPP = tetraphenylporphyrin),[26] leading to an enhancement of totally symmetric modes that are mainly derived from A_{1g} symmetry. Three major RR bands such as the ν_2 mode at 1544 cm^{-1}, ν_4 mode at 1354 cm^{-1}, and ν_6 mode at 1003 cm^{-1} were observed in the high-frequency region. The Raman mode assignment of the monomer was made on the basis of the reported one of Ni^{II}TPP[27] and summarized in Table 1. It is noteworthy that the Raman modes related to meso-phenyl groups in Zn^{II}TPP,[26c] such as the ϕ_4 (ν(phenyl)) mode at 1600 cm^{-1} and ν_1 ($\nu(C_mC_{ph})$) mode at 1238 cm^{-1}, were not much enhanced in the Raman spectrum of Z1. A distinct difference in the enhancement pattern of the phenyl-related Raman modes is attributable to the bulky and heavier 3,5-dioctyloxyphenyl group substitution at meso positions of the constituent porphyrin monomer, which hinders the rotation of the phenyl ring from vertical conformation to the porphyrin ring plane. This feature becomes evident from a large enhancement of the ϕ_4 and ν_1 modes in the Raman spectra of Z1′ and Z2′, in which the peripheral group is the phenyl ring without bulky octyloxy chains (Figure 6).

The RR spectra of Z2, Z3, and Z4 with photoexcitation at 416 nm, which is in resonance with the high-energy Soret bands in the arrays, resemble that of their constituent porphyrin monomer except for a slight variation in the enhancement of some RR bands (Figure 4a). Considering the monomeric features of the high-energy Soret band, the Raman bands of the porphyrin arrays by photoexcitation at the high-energy Soret bands are regarded to originate predominantly from the in-plane porphyrin ring skeletal modes localized on the monomeric porphyrin ring. The similarity in the in-plane porphyrin ring skeletal modes between the constituent monomer porphyrin and its arrays indicates that the porphyrin macrocycle structure remains intact

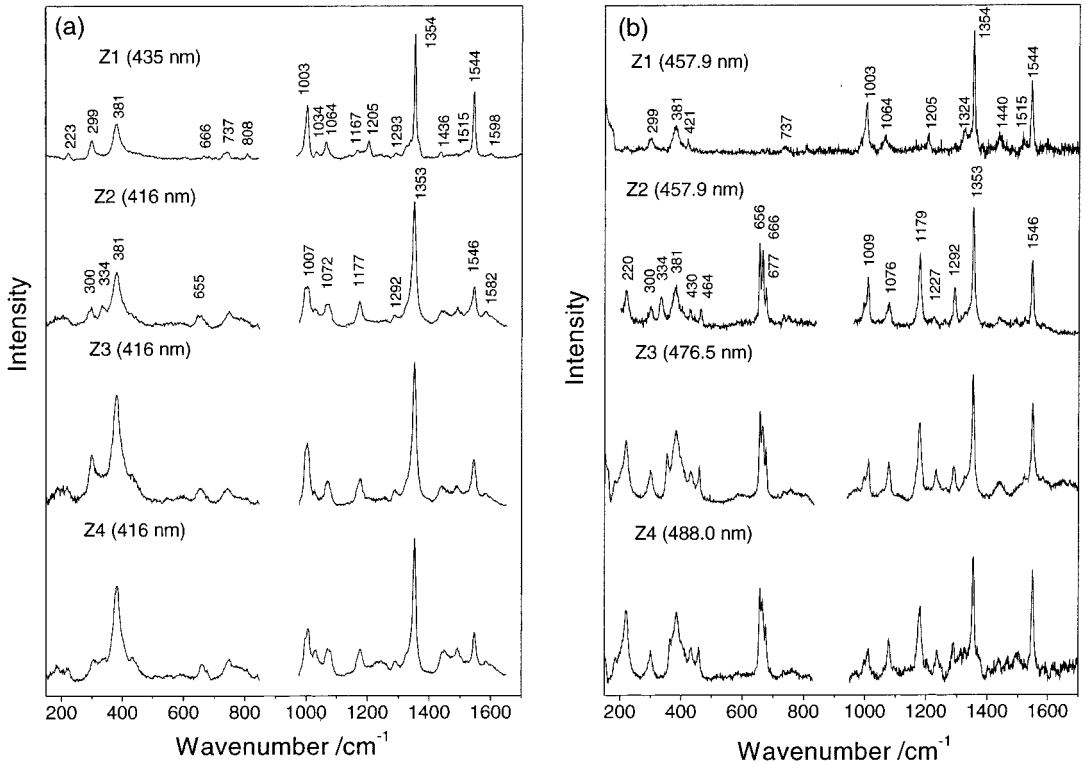

Figure 4. (a) Resonance Raman spectrum of Z1 with the B-band excitation, and those of Z2, Z3, and Z4 with excitations at their high-energy Soret bands. (b) Raman spectrum of Z1 with 457.9 nm excitation and those of Z2, Z3, and Z4 with excitations at their low-energy exciton split Soret bands.

TABLE 1: Normal Modes of Porphyrin Monomer, Z1

local coordinate			Z1 (obs)	Z1′ (obs)	^{13}C−Z1′ (obs)	Z1′ (calc)	Zn^{II}TPP (calc)	Ni^{II}TPP (obs)[27a]
ν_{18}	ν(N−M)	B_{1g}	223	223		197	208	277
ϕ_{10}	ν(Por-Ph)[a]	A_{1g}	299	313	313	327	212	202
ν_8	ν(NM)	A_{1g}	381	390	389.5	396	396	402
ϕ_9	$\delta(C_\alpha C_m C_\alpha) + \nu_{6a}$(Ph)	B_{2g}	666	647	645	631	619	639
ν_{16}	δ(Pyr deform)$_{sym}$	B_{1g}	738	788	787.5	784	798	846
ν_7	δ(Pyr deform)$_{sym}$	A_{1g}		879	878.5	863	872	889
ν_6	ν(Pyr breath)	A_{1g}	1003	995	994.5	959	961	1004
ν_{30}	ν(Pyr breath)	B_{2g}	∼1003	1001	1001	1081	1031	998
ν_{17}	ν_{18a}(Ph)	B_{1g}	1034	1025	1024		1079	1079
ν_9	$\delta(C_\beta H)_{sym}$	A_{1g}	1064	1068	1068	992	1007	1079
ν_1	$\nu(C_m C_{phenyl})$	A_{1g}	1205	1260	1246	1290	1310	1235
ν_{29}	ν(Pyr quarter)	B_{2g}	1324			1333	1342	1377
ν_4	$\nu(C_\alpha C_\beta)+\nu(NC_\alpha)$	A_{1g}	1354	1355	1355	1340	1339	1374
ν_3	$\nu(C_m C_\alpha)_{sym}$	A_{1g}	1438	1439	1437	1471	1468	1470
ν_2	$\nu(C_\alpha C_m) + \nu(C_\beta C_\beta)$	A_{1g}	1544	1546	1543	1496	1498	1572
ϕ_4	ν_{8a}(Ph)	A_{1g}	1594	1599	1599	1605	1611	1599

[a] Por, Ph, and Pyr indicate porphyrin, phenyl, and pyrrole, respectively. The notations for normal mode classification are adapted from ref 27a.

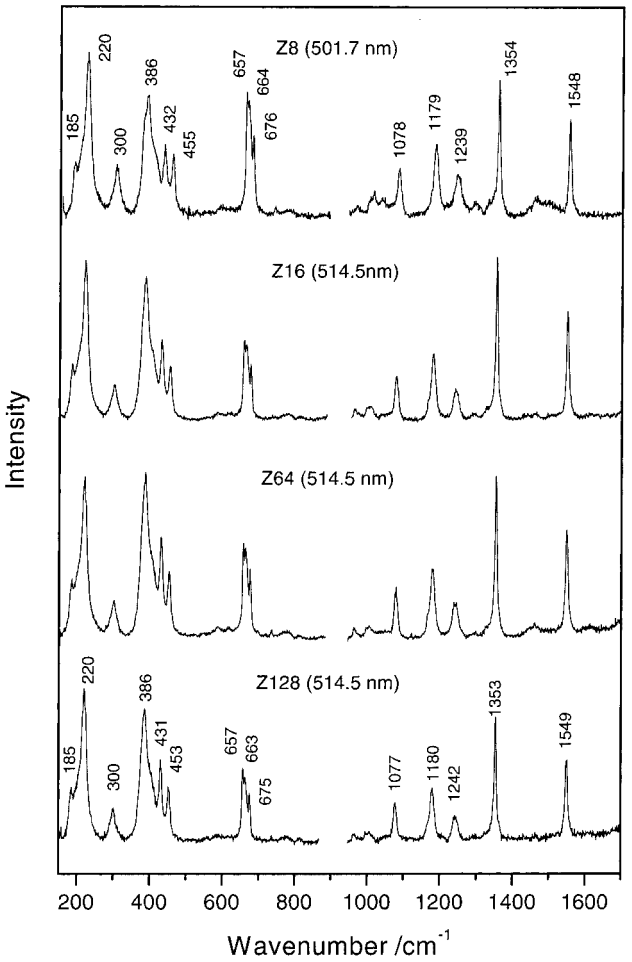

Figure 5. RR spectra of Z8, Z16, Z64, and Z128 with excitations at their low-energy exciton split Soret bands.

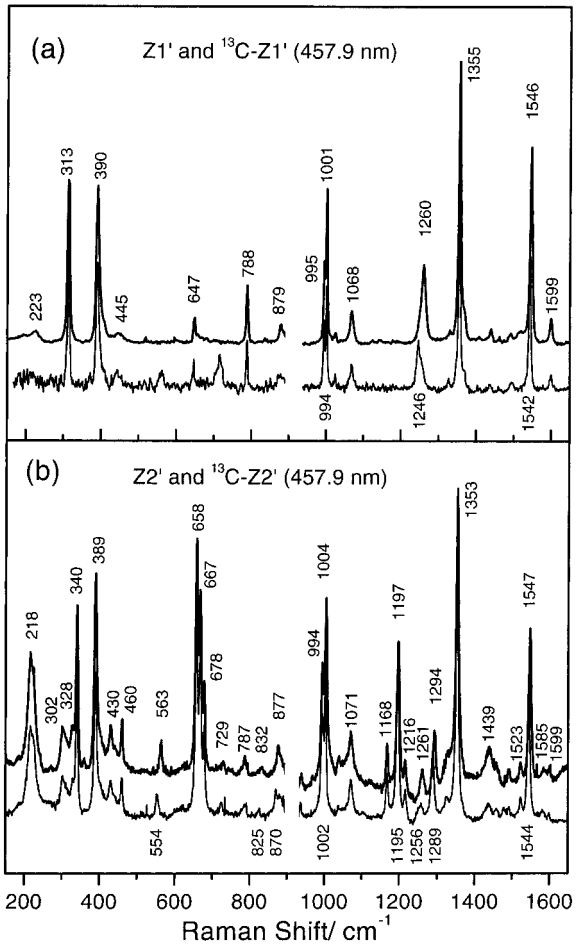

Figure 6. (a) Raman spectra of Z1 (top) and its ^{13}C isotope substituted analogue (bottom) with 457.9 nm excitation. (b) RR spectra of Z2 (top) and its ^{13}C isotope substituted analogue (bottom) with 457.9 nm excitation.

as 3,5-dioctyloxyphenyl substituents are employed to enhance the solubility of longer arrays.

On the other hand, the overall RR enhancement pattern of the porphyrin arrays with excitation at the low-energy exciton split Soret bands become complicated, being distinctly different from that of monomer (Figure 4b). The unique feature in the dimer is the appearance of RR bands at around 220, 334, 430, 464, 1179, and 1292 cm^{-1} in addition to the closely positioned three Raman bands in the vicinity of 650−680 cm^{-1}. The overall features of the dimer RR spectra are summarized in Table 2. Furthermore, this spectral feature constantly appears in the RR spectra of all the porphyrin arrays, even in Z128 (Figure 5). It is of interest to observe that the RR bands at 220, 430, and 464 cm^{-1} gain in their intensities with increasing array sizes. The RR bands at 334, 464, and 1227 cm^{-1} in the dimer exhibit a systematic shift in frequency with an increase in the number of porphyrin units in the arrays accompanied by a gradual increase in their relative intensities (Figure 7). The frequency shifts converge to their limiting values when the number of porphyrin units reaches around six. The asymptotic frequency shifts of the RR bands is reminiscent of that of the phonon modes of

TABLE 2: Normal Modes of Porphyrin Dimer, Z2

local coordinate				Z2 (obs)	Z2′ (obs)	^{13}C−Z2′ (obs)	Z2′ (calc)	ρ^a	Z1
ν_{35}	ν(Pyr-transl)	$B_{2g}{}^b$	antisym	185			131		[132]^c
			sym	220	218	218	166	0.34	
ϕ_{10}	ν(por-ph)	A_{1g}	antisym	300	302	302	328	0.35	299
			sym	334	340	340	339	0.35	
ν_8	ν(NM)	A_{1g}	both	381	389	389	395	0.36	381
ν_{33}	ν(Pyr rot)	B_{2g}	antisym				411		421
			sym	430	430	429.5	435	0.42	
ν_{49}	ν(Pyr rot)	A_{1g}	antisym				463		498
			sym	464	460	459.5	492	0.25	
ϕ_9	$\delta(C_\alpha C_m C_\alpha) + \nu_{6a}$(Ph)	A_{1g}	antisym	656	658	658	632	0.30	666
			sym	677	678	678	647	0.30	
ϕ_9''	$\delta(C_\alpha C_m C_\alpha) + \nu_{6a}$(Ph)	E_u	both	666	667	667	642	0.33	
ν_6	ν(pyr breath)	A_{1g}	both	1009	1004	1002	958	0.33	1003
ν_9	$\delta(C_\beta H)_{sym}$	A_{1g}	antisym	1072			991		1064
			sym	1076	1071	1071	994	0.33	
ν_{34}	$\delta(C_\beta H)_{asym}$	B_{2g}	sym		1168	1168	1133		1167
			antisym	1177			1150		
ν_{51}	$\delta(C_\beta H)_{asym}$	E_u	sym	1179	1197	1196	1181	0.32	
			antisym		1216	1216	1186		
ν_1	$\nu(C_m C_{phenyl})$	A_{1g}	antisym				1289		1205
			sym	1227	1261	1256	1304	0.38	
ν_{27}	$\nu(NC_\alpha) + \nu(C_m C_{phenyl})$	B_{2g}	antisym				1331		
			sym	1292	1294	1289	1346	0.28	
ν_4	ν(pyr half-ring)$_{sym}$	A_{1g}	both	1353	1353	1353	1374	0.36	1354
ν_2	$\nu(C_\beta C_\beta)$	A_{1g}	both	1546	1547	1544	1572	0.34	1544

^{a} Depolarization ratio defined by $\rho = I_\perp/I_\parallel$. ^{b} Symmetry block in D_{4h} symmetry. ^{c} Number in bracket is calculated value.

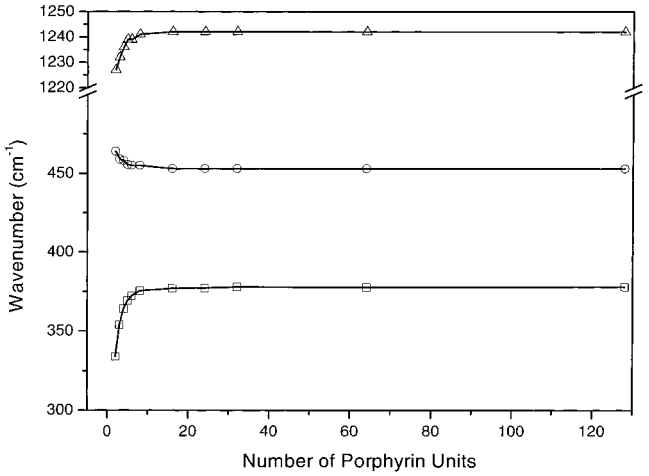

Figure 7. Plot of vibrational frequency shifts of the ϕ_{10}, ν_{49}, and ν_1 modes vs number of porphyrin units in the arrays: squares for ϕ_{10}, circles for ν_{49}, and triangles for ν_1.

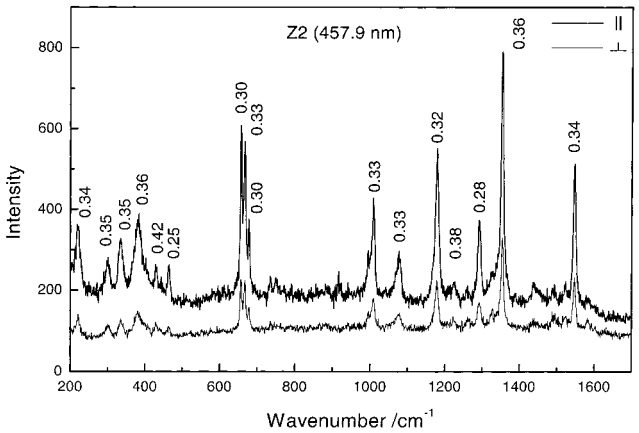

Figure 8. RR spectra of Z2 with excitation at the low-energy exciton split Soret band. The top and bottom ones correspond to parallel (||) and perpendicular (⊥) polarizations, respectively.

polymers with an increase of the polymer length.[28] On the other hand, the RR band at 1292 cm^{-1} is gradually diminished as the number of porphyrin units increases. Newly observed RR bands in the dimer at 1179 cm^{-1} and in the 650−680 cm^{-1} region retain their peak positions with increasing array sizes.

The RR spectra of Z1′ and Z2′ and their isotope-substituted analogues were also measured in order to obtain the Supporting Information for the normal-mode analysis of Z2 and longer porphyrin arrays (Figure 6). The ν_1 and ν_2 modes of Z1′ show large shifts by ^{13}C isotope substitution, which is consistent with that of Ni^{II}TPP.[27a] The frequency shift in the RR spectrum of Z2 by ^{13}C isotope substitution was found in several bands that were not observed in the Raman spectrum of Z1. This feature was utilized in assigning the RR bands of Z2, especially for the involvement of 5 and 15 meso-carbons connecting peripheral groups. For instance, the new Raman bands at 1197 and 1294 cm^{-1} in the RR spectra of Z2′ exhibit conspicuous frequency shifts by isotope substitution, but the strong triple bands at around 660 cm^{-1} do not show any shift.

Depolarization ratios for the RR bands of Z2 were also examined to characterize their symmetry properties (Figure 8). For the RR bands with considerable intensities the depolarization ratios are given to be around 0.3. Even the RR bands that are assigned to the totally symmetric modes of the porphyrin monomer with D_{4h} symmetry show depolarization ratio values ranging from 0.33 to 0.38. These values are summarized in Table 2.

Normal-Mode Analysis of Dimer. Normal mode calculation was carried out in the level of AM1 calculation. With the aid of experimental isotope RR data of the dimer, we try to determine the origins of vibrational modes with the current calculation based on the following steps. First, we performed the normal mode calculation of Zn^{II}TPP of which structure is similar to Ni^{II}TPP and compared it with that of Ni^{II}TPP[27] to estimate a correlation factor related to the change of the central metal and the difference of calculation method. Second, we compared the normal modes of Zn^{II}TPP with the calculated normal modes of Z1′ since the normal modes of Z1′ would be intrinsically distorted from those of Zn^{II}TPP due to the symmetry reduction. Third, the normal modes of Z2′ were calculated and

compared with those of Z1′. Fourth, the RR experiments of the porphyrins (Z1′ and Z2′) isotope-labeled at 5 and 15 meso-carbons were utilized to confirm the assignment at least for the limited number of Raman bands. These sequential procedures enabled us to find the origins of normal modes of the dimer. In fact, the constituent monomer unit in the arrays is DPP-type (diphenylporphyrin) and hence, its vibrational eigenvectors corresponding to TPP-type (tetraphenylporphyrin) porphyrin will be more or less perturbed, and the dimeric interaction in the dimer also induces further perturbation to the normal modes. This feature precludes an assignment of the normal modes of the DPP-type porphyrin dimer based on those of TPP-type porphyrin monomer. Nevertheless, according to the current calculation, the individual normal modes of the dimer (Z2) still maintained the fundamental characters of normal modes of TPP-type porphyrin monomer that are well-known in the literature. In all the calculations, we did not include dioctyloxy chains attached to phenyl meta positions. The geometry of each monomer unit was proposed to be planar (D_{2h} symmetry) because no band characteristic of nonplanar porphyrins[29] was observed in our RR spectra of the arrays.

1. Porphyrin Monomer (Z1). Most of Raman bands in Figure 4a,b correspond to the A_{1g} block of porphyrin monomer. However, a few nontotally symmetric modes (B_{1g} and B_{2g}) of weak intensities were observed. The B_{1g} and B_{2g} modes show different features under D_{2h} symmetry for the monomer and D_{2d} symmetry for the dimer. B_{2g} modes become totally symmetric A_g modes under D_{2h} symmetry and also produce totally symmetric A_1 modes in Z2. B_{1g} modes in D_{4h} symmetry become nontotally symmetric modes (B_{1g}) when the symmetry is degraded to D_{2h} symmetry (Z1). B_{1g} modes cannot build totally symmetric vibrational modes of Z2 under D_{2d} symmetry and, thus, disappear in Z2 by photoexcitation at the low-energy Soret band. That is the reason that B_{1g} modes can gain their intensities, even if weak, in Z1. The band at 738 cm^{-1} in the Raman spectrum of Z1 is assigned to the B_{1g} mode (ν_{16}) because it appears with considerable intensity in the Raman spectrum of Z1 but loses its intensity in the RR spectrum of Z2 by the low-energy Soret excitation. A consistent feature is observed in the RR spectra of Z1′ and Z2′, where the corresponding band at 788 cm^{-1} becomes weak in the dimer. The bands at 223 and 1034 cm^{-1} are assigned to this symmetry block (ν_{18} and ν_{17}, respectively). The 1034 cm^{-1} band was observed in the dimer RR spectrum by the high-energy Soret excitation but was conspicuously diminished in the RR spectrum by the low-energy Soret excitation that shows dimeric features. The band at 223 cm^{-1} in the RR spectra of Z1 behaves like a B_{2g} mode since it gains intensity in the RR spectrum of Z2 by the low-energy Soret excitation. However, no modes of A_{1g} or B_{2g} symmetry falling near 223 cm^{-1} were found from the normal mode calculation of Z1, but the ν_{18} mode of B_{1g} symmetry was calculated to appear at 197 cm^{-1}. The ν_{18} mode is the most probable candidate in consideration of vibration frequency but cannot explain an enhancement of the band at 220 cm^{-1} observed in the RR spectrum of Z2 by the low-energy Soret excitation. Thus, the 223 cm^{-1} band in the Z1 Raman spectrum is assigned to the ν_{18} mode, but the intense band at 220 cm^{-1} in the Z2 RR spectrum by the low-energy Soret excitation is assigned to another mode composed of dimeric interaction of the ν_{35} mode, falling coincidentally at this position (vide infra).

The effect of removing two heavy peripheral groups from TPP structure is pronounced in the ϕ_{10} and ν_{16} modes that involve the movement of phenyl groups. The calculated frequency of the ϕ_{10} mode of Zn^{II}DPP is ~110 cm^{-1} higher than that of Zn^{II}TPP, and the ν_{16} mode of Zn^{II}DPP was calculated to be ~60 cm^{-1} lower in frequency than that in Zn^{II}-TPP. Hence, the ϕ_{10} and ν_{16} modes of Z1 are assigned to 299 and 738 cm^{-1}, respectively even though the ϕ_{10} and ν_{16} modes of Ni^{II}TPP appear at 202 and 846 cm^{-1}, respectively. Distortion of eigenvectors of normal modes from Ni^{II}TPP occurs in some modes of Z1 due to the symmetry reduction from D_{4h} to D_{2h}. The ν_8, ν_{16}, ν_7, ν_1, and ν_4 modes correspond to this case. This prevents the direct assignment of these modes by comparison of normal mode eigenvectors. The assignment of the ν_1 and ν_2 modes is confirmed by the frequency shift of the isotope labeled porphyrin, ^{13}C-Z1′, since these modes involve the movement of meso-carbons (i.e., $\nu(C_mC_{phenyl})$ and $\nu(C_\alpha C_m)$, respectively). The band at 1003 cm^{-1} is a superposition of two modes, ν_6 and ν_{30}. The two modes are not resolved in Z1 but they are well resolved in Z1′ due to a slight difference in peripheral groups.

The very weak band at 666 cm^{-1} in the Z1 Raman spectrum is assigned to the ϕ_9 mode. The ϕ_9 mode is a probable choice because it appears at 639 cm^{-1}. The 666 cm^{-1} band that is very weak in the Z1 Raman spectrum becomes strong and split into three bands appearing at 656, 666, and 677 cm^{-1} in the RR spectrum of Z2 by the low-energy Soret excitation.

2. Porphyrin Dimer (Z2). Normal mode calculation of Z2′ reveals that a number of vibrations occur in a localized manner such as vibrations in a single porphyrin ring and in a single phenyl ring and a smaller number of vibrations occur in a delocalized manner throughout two porphyrin rings. In the latter case, eigenvectors of the vibrational modes exhibit that they are composed of symmetric and antisymmetric combinations of monomer vibrational modes. The delocalized vibrational modes are further classified into two cases. One is that the symmetric and antisymmetric vibrational modes are degenerate and are expected to occur as one band. The other is that they are not degenerate but split into two. Interestingly, most of the vibrations that fall in the A_{1g} block in the porphyrin monomer yield the degenerate vibrations in Z2′ (Table 2 and Figure 9). The splitting of the combination modes occurs in the vibrations of B_{2g} and E_u symmetry. The B_{2g} and E_u modes are not totally symmetric in porphyrin monomer but become totally symmetric with A_1 symmetry in the porphyrin dimer of D_{2d} symmetry by a symmetric combination of monomer vibrations (Figure 10). Normal mode assignment of Z2 is summarized in Table 2 where the observed and calculated frequencies of Z2′ and those of porphyrin monomer are also compared. Our assignment was compared with that by Bhuiyan et al. for a similar porphyrin complex[30] showing a disagreement for a few bands. Especially, we can extend the assignment for the low-frequency modes below 1000 cm^{-1}, which is not available in the literature.

Several bands were found to include contributions from phenyl group movements. The ν_{35} (B_{2g}) and ϕ_{10} (A_{1g}) modes are especially of interest because the phenyl group moves as a single vibrating unit.[27a,31] By excitation of the low-energy Soret transition the band at 220 cm^{-1} in the RR spectrum of Z2 shows a gradual increase in intensity as the number of porphyrin units increases, but by excitation of the high-energy Soret transition this band becomes very weak. This reflects that the 220 cm^{-1} band is characteristic of dimer interaction. Therefore this band is assigned to the symmetric combination band of the ν_{35} mode of Z1 (Figure 11). The band appearing at 185 cm^{-1} as a shoulder of the 220 cm^{-1} band from Z3 is assigned to the antisymmetric combination band of the ν_{35} mode of Z1. These modes show no frequency shift by isotope substitution even if they involve meso-carbon movement. This can be attributed to the fact that

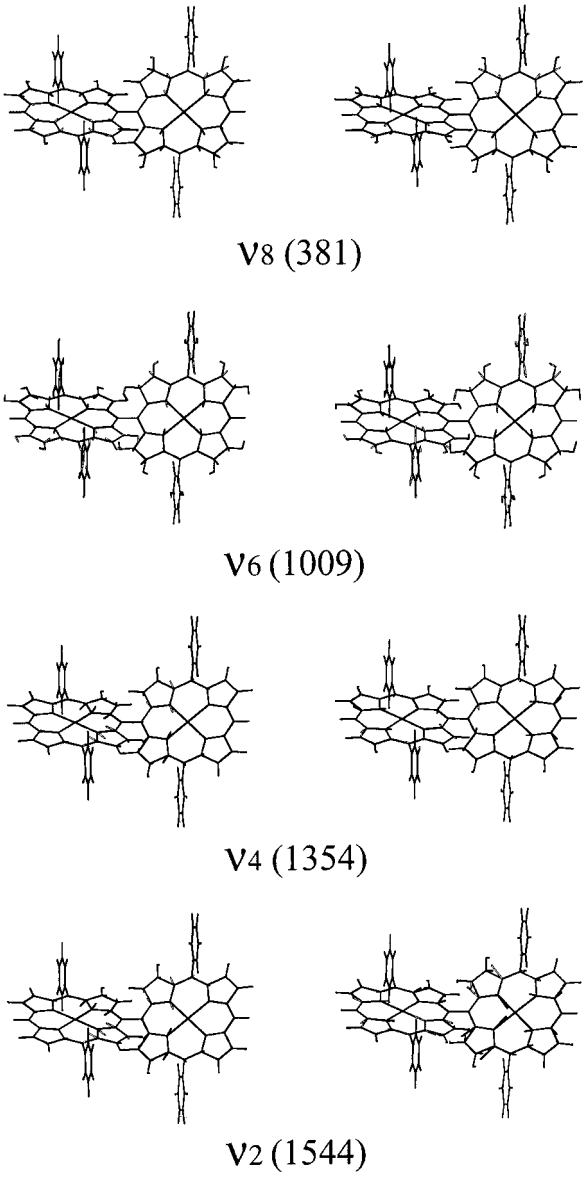

Figure 9. Vibrational eigenvectors of the Raman modes of Z2′ showing degenerate combination modes. The left are antisymmetric combinations and the right are symmetric ones.

meso-carbons move in-phase with the phenyl group and thus no internal stretching occurs between the meso-carbon and phenyl group. Similar splitting by antisymmetric and symmetric combinations of ϕ_{10} (A_{1g}) and ϕ_{10}'' (E_u) modes is anticipated, but only those of ϕ_{10} mode were found in the normal mode calculation of Z2′. Therefore, the bands at 300 and 334 cm^{-1} are assigned to the antisymmetric and symmetric combination bands of the ϕ_{10} mode, respectively.

The triple bands at around 660 cm^{-1} are a characteristic feature of dimer interaction since they are very weak or not observed in the RR spectra of Z1 and Z2 by photoexcitation at the high-energy Soret transition, but become very strong in the RR spectrum of Z2 by photoexcitation at the low-energy Soret transition. They are assigned to the combination of ϕ_9 (A_{1g}) and ϕ_9'' (E_u) modes (Figure 10). The combination pair of the ϕ_9'' mode is calculated to be degenerate. Even if the ϕ_9 and ϕ_9'' modes involve phenyl in-plane vibrations, equivalent contribution from porphyrin in-plane motions is included simultaneously. If the ϕ_9 and ϕ_9'' modes are dominantly composed of phenyl modes, an enhancement of three bands at 656, 666, and 677 cm^{-1} is ascribed to increased $\pi-\pi$ resonance between phenyl and porphyrin rings. Then, a similar enhancement of the ϕ_{10} mode at ~1600 cm^{-1}, which is characteristic of $\pi-\pi$ resonance of phenyl and porphyrin rings, is expected but it is not the case. The enhancement of these bands is attributed to the porphyrin in-plane motions and the phenyl group is regarded to contribute as a single vibrating mass depending on its internal mode as such as in ϕ_{10} mode. The combination bands of ϕ_9'' modes is not truly the combination of two ϕ_9'' modes of both porphyrin monomers, but that of one ϕ_9'' mode from one porphyrin unit and one out-of-plane mode ($\gamma(NC_\alpha C_m)_{sym}$) from the other porphyrin unit (Figure 10).

The ν_8, ν_6, ν_4, and ν_2 modes that fall in the A_{1g} symmetry block in the porphyrin monomer have different characteristics from the above-mentioned modes. Normal mode calculation of Z2 reveals that these modes are composed of symmetric and antisymmetric combination modes but they are degenerate in frequency (Table 2). However, it is not the case for all A_{1g} modes since the ν_9 and ν_1 modes show the splitting of their combination modes. The other porphyrin in-plane modes such as ν_{35}, ν_{33}, ν_{34}, ν_{51}, and ν_{27} modes of B_{2g} or E_u symmetry show splitting in calculation. These modes are of importance because their symmetric combination modes involve the vibration of meso−meso-carbons linking two porphyrin rings. They correspond to the bands at 220, 334, 430, 464, 1179, and 1292 cm^{-1} for the ν_{35}, ϕ_{10}, ν_{33}, ν_{49}, ν_{51}, and ν_{27} modes, respectively. Among them the low-frequency modes are composed of pyrrole rotation or translational motion in phase with meso-carbon movement. Especially in the symmetric combination mode of the ϕ_{10} mode, four pyrrole rings undergo translation motion in phase with the meso-carbon, and hence, each porphyrin unit behaves as a single vibrating unit, such as the phenyl group in the ϕ_{10} mode of porphyrin monomer. On the other hand, the meso−meso-carbon stretching of the ν_{51} and ν_{27} modes involves pyrrole asymmetric half-ring motion in addition to asymmetric $C_\beta-H$ motion in which $\nu(C_m-C_m)$ vibration is mixed with $C_\alpha C_m C_\alpha$ bending motion (Figure 10). This internal vibration near the meso-carbon does not appreciably affect the $\nu(C_m-C_m)$ vibration as in the case of the ϕ_{10} mode and makes it occur in the high-frequency region. The assignment of ν_{49}, ν_{51}, and ν_{27} modes are further supported by the isotope experiment. The ν_{27} mode is easily assigned on the basis of the large shift of the 1294 cm^{-1} band in the Raman spectrum of Z1′ due to the $\nu(C_mC_{phenyl})$ contribution to this mode. Even though the ν_{51} mode is characterized by $\delta(C_\beta H)_{asym}$, it has considerable contribution of C_m-phenyl movement, as shown in Figure 10. This mode is thus assigned to the 1179 cm^{-1} band (1197 cm^{-1} in Z2′) that shows an isotope shift in frequency. The ν_{49}, ϕ_9, and ϕ_9'' modes that apparently have contribution from the phenyl group are assigned to the bands that do not show isotope shift. However, referring to the eigenvectors of the modes, we can find that C_m and C_{phenyl} are moving in-phase or their displacements are very small.

IV. Discussion

The resonance Raman scattering theory predicts that the vibrational modes enhanced via the *A*-term (or Franck−Condon scattering) are dominant when the laser frequency is in resonance with a strongly allowed electronic transition, and the vibrational modes enhanced via the *B*-term (or Herzberg−Teller term) prevail when the laser frequency is in resonance with a weakly allowed electronic transition in a molecular system where there is a nearby very strong transition.[32] Under the D_{4h} symmetry of a monomeric porphyrin, in-plane porphyrin skeletal vibrational modes are classified as totally symmetrically polarized A_{1g}, depolarized nontotally symmetric B_{1g} and B_{2g} and finally

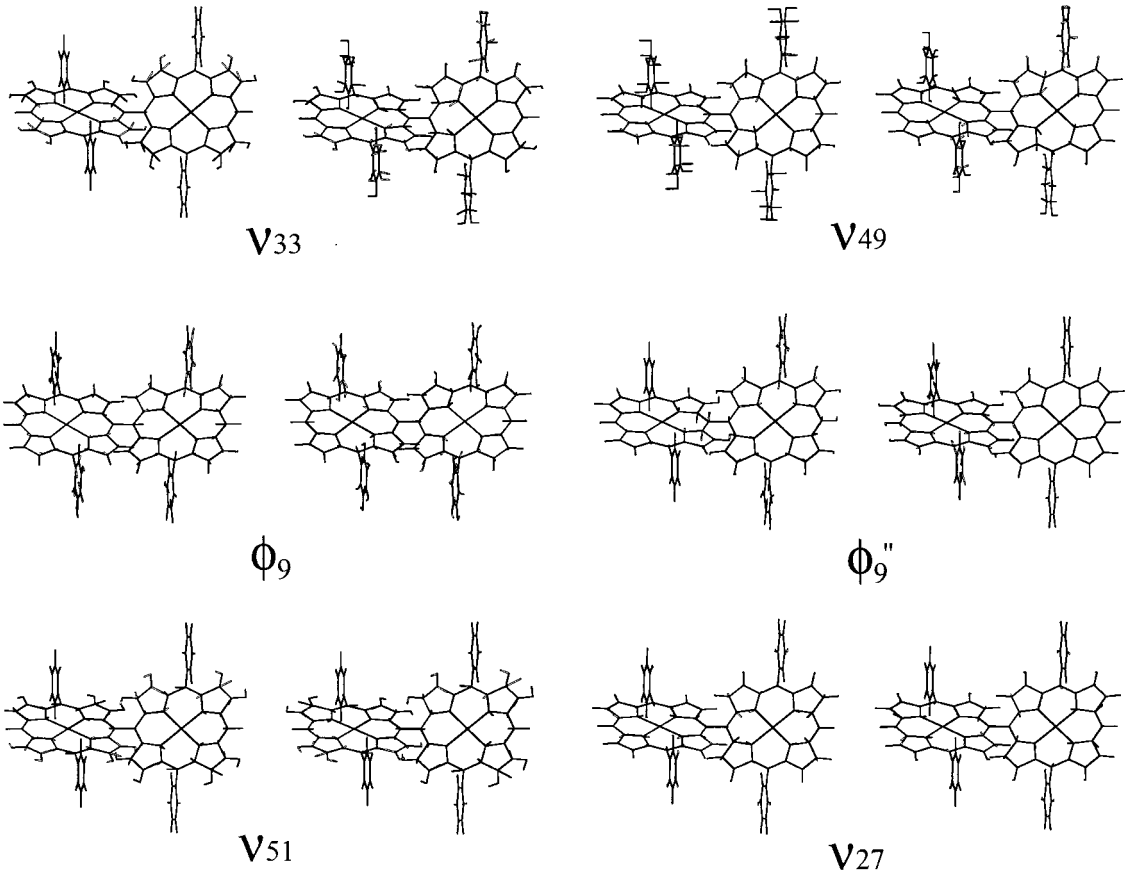

Figure 10. Vibrational eigenvectors of the Raman modes of Z2′ that show splitting between antisymmetric (left) and symmetric (right) combination modes of the monomeric Raman modes.

anomalously polarized A_{2g} modes.[33] It is well established that for monomeric porphyrins totally symmetric modes are predominantly enhanced upon photoexcitation at the Soret band. On the other hand, Q-band excitation of porphyrins yields the RR spectra mainly composed of nontotally symmetric modes.

The RR spectra of the arrays with excitation at the high-energy Soret bands exhibit predominantly monomeric features (Figure 4a). This is related to the monomeric character of the high-energy Soret band with no excitonic interaction due to the orthogonal geometry.[16] Most of the RR bands enhanced by the high-energy Soret transition are originated from the totally symmetric modes of porphyrin monomer such as ν_8, ν_6, ν_4, and ν_2 modes. Their corresponding eigenvectors exhibit symmetric and antisymmetric combinations of such modes but the combination modes are degenerate in frequency. This implies that each vibrating unit behaves independently even if the overall shape of the eigenvectors forms a symmetric or antisymmetric combination. Then, the RR process of the arrays by photoexcitation at the high-energy Soret transition should be described as occurring locally at each porphyrin unit. In the RR process by photoexcitation at the high-energy Soret band, the effective symmetry of the dimer would be D_{4h} (or D_{2h}), such as Z1, even though the arrays have different symmetry, such as D_{2d} for the dimer.

The RR spectra of the arrays obtained by excitation at the low-energy bands reveal new RR bands at 334, 430, 464, 656, 666, 677, 1179, and 1292 cm^{-1} that were not observed in the RR spectrum of monomer (Figure 4b). Most of them are originated from the nontotally symmetric modes of porphyrin monomer. These modes may derive their intensities from the *B*-term scattering because the strong high-energy Soret band is located very close and its oscillator strength is large. However, the low-energy exciton split Soret bands are also very intense compared to the high-energy Soret bands and, accordingly, the *A*-term contribution also can substantially contribute to the RR enhancement. This seems to sustain a delicate balance between the *A*- and *B*-term contributions.[34]

The depolarization ratio values for the arrays were measured to obtain further information on the origin of RR enhancement (Figure 8). For a planar scatter with the D_{4h} symmetry group, the depolarization ratio, ρ, is expected to be 0.125 for totally symmetric A_{1g} modes where $\alpha_{xx} = \alpha_{yy} \neq 0$ and $\alpha_{zz} = 0$ for the diagonal polarizability tensor elements.[35] The B_{1g} and B_{2g} modes are depolarized with $\rho = 0.75$. However, for a nonplanar scatter with the D_{2d} symmetry group, the depolarization value is expected to be $0 \leq \rho \leq 0.75$ for totally symmetric A_1 modes where $\alpha_{xx} = \alpha_{yy}$ ($\neq 0$) $\neq \alpha_{zz}$ ($\neq 0$).[36] Most of the depolarization ratio values of the RR bands of Z2 shown in Figure 7 turn out to be around 0.33. This is a drastic change in the depolarization ratios of the RR bands. The change of depolarization ratios, especially in the RR bands assigned to the A_{1g} modes, seems to be inconsistent with the monomeric features in the RR spectrum of Z2 by photoexcitation at the high-energy Soret band. This implies that different symmetries would be applied to Z2 for the photoexcitations at the two Soret bands. Similar depolarization ratios for the RR bands of Z2 irrespective of their inherent symmetry of constituent porphyrin unit (A_{1g}, B_{2g}, or E_u) reflect that these RR bands correspond to the same symmetry block or A_1 under D_{2d} symmetry and are RR enhanced by the same mechanism. If we regard the depolarization ratios of ~0.33 to be characterisitic of porphyrin dimer (Z2), the *A*-term enhancement mechanism is likely to prevail. For longer arrays, the depolarization ratio values were measured to be almost the same as that of Z2.

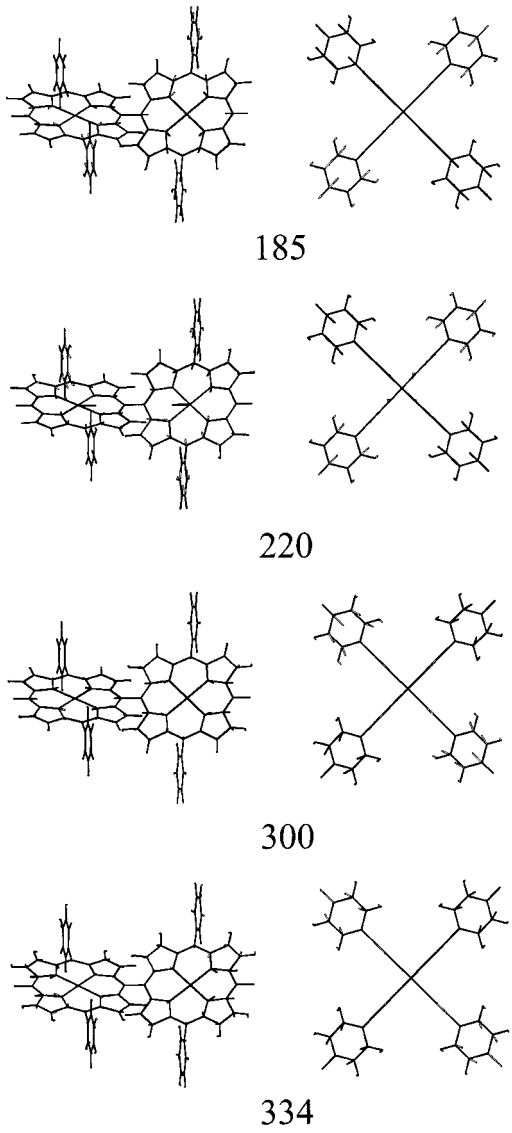

Figure 11. Vibrational eigenvectors of the ν_{35} and ϕ_{10} modes of Z2′. The right ones are side views showing phenyl ring movement as a single vibrating unit.

In a dimeric system, a couple of new vibrational modes could show up by the combination of vibrational modes from both monomer units: one is symmetric vibration and the other is an antisymmetric one.[37,38] When the dimeric coupling is weak, these two vibrations remain degenerate, and concomitantly, appear as one band, just like the vibrational spectrum of the monomer. On the other hand, as the dimeric coupling becomes pronounced, the two vibrations become split into separate bands.[19] Then, the frequency of each vibration appears shifted from that of monomer. The porphyrin dimers, especially sandwich complexes that are axially bridged either via direct metal−metal bonds[18] or via single atoms such as oxygen and nitrogen,[17] have been extensively studied by RR spectroscopy because of their potential utility as a model system for probing *intra*dimer coupling between closely spaced porphyrin units. However, the dimer splitting has not been observed in the sandwich-type porphyrin dimers, especially even in the multiply metal−metal-bonded porphyrin dimers with a metal−metal bond distance of ∼2.2 Å. In the case of Z2, the distance between the adjacent porphyrin rings is very close (ca. 1.4 Å) even though the center-to-center distance is 8.35 Å. Owing to the significantly reduced distance, the *intra*dimer vibrational splitting via excitonic interactions is expected.

Through the symmetry reduction from D_{4h} to D_{2d} or D_2 by dimerization, nontotally symmetric modes in the monomer unit could become totally symmetric ones. The modes with A_{1g}, B_{2g}, and E_u symmetries in the monomer (D_{4h}) become totally symmetric modes in the dimer (D_{2d}) by a proper combination of the vibrations of each monomer unit: $A_{1g} \rightarrow A_1$, B_2; $B_{2g} \rightarrow A_1$, B_2; $E_u \rightarrow A_1$, B_2, E. The symmetric combination of these modes builds A_1 modes and the antisymmetric combination does B_2 modes. The observed new RR bands are assigned to the totally symmetric A_1 modes. The B_2 modes that span *xy*-quadratic and *z* components are both Raman and IR active but are not RR enhanced by photoexcitation at the low-energy Soret band. Because of these symmetry properties the observation of split bands, if any, is not probable in the RR spectrum. The antisymmetric combination bands of B_2 symmetry are expected to appear in the IR spectrum or in the RR spectrum by photoexcitation at Q-bands through the Herzberg−Teller vibronic borrowing mechanism. Unfortunately, the RR spectrum of Z2 by Q-band excitation could not be obtained because of strong fluorescence. The IR spectrum of Z2 was not helpful due to too many overlapped bands from porphyrin and phenyl rings. However, normal mode calculation exhibits the existence of vibrational splitting of the RR bands: one is the symmetric combination mode with A_1 symmetry and the other is the antisymmetric combination mode with B_2 symmetry (Table 2). According to the calculation, not all the vibrational modes of porphyrin monomer show vibrational splitting. The B_{2g} and E_u modes including a few A_{1g} modes become split by dimeric interaction. The ν_{35}, ϕ_{10}, ν_{33}, ν_{49}, ϕ_9, ν_{51}, and ν_{27} modes correspond to this case. Most of the A_{1g} modes do not appear to split. The eigenvectors of the Raman bands originated from the B_{2g} and E_u modes of porphyrin monomer are perturbed from their monomeric eigenvectors but those from the A_{1g} modes appear to maintain the shapes of their monomeric analogues. The latter seems to be related to the enhancement of only the totally symmetric modes by photoexcitation at the high-energy Soret band.

Vibrational splitting in the dimer is directly related to the buildup of optical phonon modes of the arrays. If there is no vibrational splitting in the dimer and, accordingly, in the longer arrays, the vibrational frequencies of the arrays would be the same as those of the constituent monomer. Then, the optical phonon modes could not be built up with the constituent internal vibration modes of monomers. We could find some Raman bands that show phonon-like characters of polymers.[28] As the number of porphyrin units increases, gradual frequency changes for a few Raman bands such as the ϕ_{10}, ν_{49}, and ν_1 modes were observed, as shown in Figure 7. The asymptotic feature of the frequency change is similar to that of *n*-paraffins' limiting phonon mode with $\varphi = \pi$ vibrations.[28] The frequency change of the Raman modes can be explained in part by the substitution environment change at meso-position from monomer to longer arrays.[28] However, this could not explain the other Raman bands that show relatively less frequency shifts such as the ϕ_9, ϕ_9'', and ν_{27} modes even though they involve meso-carbon movements.

The Raman modes that show large frequency shifts are largely related to the phenyl group movement and the C_m-C_m stretching vibration. Systematic frequency shifts are likely coupled with the RR enhancement pattern for the RR spectra of the arrays with an increase of porphyrin units. The Raman bands in the low-frequency region are largely enhanced and exceptionally the ν_1 mode shows a similar enhancement as the number of porphyrin units increases. The enhancement pattern can be rationalized by the fact that the enhanced RR bands in the low-

frequency region such as the ϕ_{10}, ν_{49}, ϕ_9, and ϕ_9'' modes and the ν_1 mode include phenyl group movement. The phenyl groups serving as heavy mass points seem to induce the porphyrin arrays to be more polarizable as the number of phenyl groups increases. The large enhancement of polarizability by phenyl groups and the C_m-C_m stretching of the ϕ_{10}, ν_{49}, and ν_1 modes are regarded to induce the phonon-like behavior of these modes. With respect to the energy transfer in the arrays, these modes may play an important role in determining a dominant pathway of energy transfer.

V. Conclusions

The close proximity and orthogonal arrangement between the adjacent porphyrins in the arrays exhibit both unshifted Soret transitions and unusually strong excitonic splitting of the Soret transitions to the red side. The RR spectroscopy revealed that by photoexcitation at the high-energy Soret bands in the arrays the Raman bands totally symmetric with respect to porphyrin monomer symmetry (D_{4h}) are activated. In contrast, excitation at the low-energy exciton split Soret bands activates the Raman bands that are totally symmetric under the symmetry of the porphyrin dimer (D_{2d}) and the longer arrays. On the basis of the normal-mode analysis using AM1 method, we assigned the RR bands characteristic of the dimer in terms of the Raman modes of porphyrin monomer. Furthermore, some of them are suggested to be evidences of vibrational splitting of porphyrin dimer based on the calculation, denoting characteristic features arising from strong excitonic interactions between the adjacent porphyrins in the arrays. The dimeric splitting in vibrational modes builds up the phonon-like vibrations in the arrays for some C_m-C_m stretching modes that show enhanced polarizability by phenyl movement as the array length increases. To obtain more direct evidence on the dimeric splitting in the Raman spectrum, further experiments such as RR measurement at the Q-band excitation using a Kerr-gating fluorescence rejection technique are required. Collectively, our investigation on the RR spectra of the porphyrin arrays combined with the normal mode calculation of the dimer has definitely promoted the understanding of the exciton coupling related to the molecular structures in the directly linked linear porphyrin arrays, which is expected to be further utilized as potential candidates for the realization of molecular photonic wires.

Acknowledgment. This work has been financially supported by the National Creative Research Initiatives Program of the Ministry of Science and Technology of Korea (D.K.). The work at Kyoto was supported by Grant-in-Aids for Scientific Research (No. 11223205 and No. 12440196) from the Ministry of Education, Science, Sports, and Culture of Japan, and by CREST (Core Research for Evolutional Science and Technology) of Japan Science and Technology Corp. (JST) (A.O.).

Note Added after ASAP Posting

This article was released ASAP on 02/07/2002 with errors in alignment of data in Table 2. The correct version was posted on 02/20/2002.

References and Notes

(1) Debreczeny, M. P.; Svec, W. A.; Wasielewski, M. R. *Science* **1996**, *274*, 584.

(2) Beljonne, D.; O'Keefe, G. E.; Hamer, P. J.; Friend, R. H.; Anderson, H. L.; Bredas, J. L. *J. Chem. Phys.* **1997**, *106*, 9439.

(3) Karki, L.; Vance, F. W.; Hupp, J. T.; LeCours, S. M.; Therien, M. J. *J. Am. Chem. Soc*. **1998**, *120*, 2606.

(4) Joran, A. D.; Leland, B. A.; Felker, P. M.; Zewail, A. H.; Hopfield, J. J.; Dervan, P. B. *Nature* **1987**, *327*, 508.

(5) Wasielewski, M. R.; Gaines, G. L., III.; Wiederrecht, G. P.; Svec, W. A.; Niemczyk, M. P. *J. Am. Chem. Soc.* **1993**, *115*, 10442.

(6) Gust, D.; Moore, T. A.; Moore, A. L. *Acc. Chem. Res*. **1993**, *26*, 198.

(7) Lin, V. S.-Y.; Therien, M. J.*Chem. Eur. J*. **1995**, *1*, 645.

(8) Osuka, A.; Marumo, S.; Mataga, N.; Taniguchi, S.; Okada, T.; Yamazaki, I.; Nishimura, Y.; Ohno, T.; Nozaki, K. *J. Am. Chem. Soc.* **1996**, *118*, 155.

(9) Strachan, J.-P.; Gentemann, S.; Seth, J.; Kalsbeck, W. A.; Lindsey, J. S.; Holten, D.; Bocain, D. F. *J. Am. Chem. Soc*. **1997**, *119*, 11191.

(10) (a) Ponomarev, G. V.; Borovkov, V.; Sugiura, K.-I.; Sakata, Y.; Shul'ga, A. *Tetrahedron Lett*. **1993**, *34*, 2153. (b) Senge, M. O.; Gerzevske, K.; Vicente, M. G. H.; Forsyth, T.; Smith, K. M. *Angew. Chem., Int. Ed. Engl*. **1993**, *32*, 750. (c) Ponomarev, G.; Borovkov, V.; Shul'ga, A.; Sakata, Y. *J. Chem. Soc., Chem. Commun*. **1994**, 1927. (d) Senge, M. O.; Vicente, M. G. H.; Gerzevske, K.; Forsyth, T.; Smith, K. M. *Inorg. Chem*. **1994**, *33*, 5625. (e) Higuchi, H.; Takeuchi, M.; Ojima, J. *Chem. Lett*. **1996**, 593.

(11) (a) Lin, V. S.-Y.; DiMagno, S. G.; Therien, M. J. *Science* **1994**, *264*, 1105. (b) Arnold, D. P.; Nitschinsk, L. *Tetrahedron* **1992**, *48*, 8781. (c) Anderson, H. L. *Inorg. Chem*. **1994**, *33*, 972. (d) Arnold, D. P.; Nitschinsk, L. *Tetrahedron Lett.* **1993**, *34*, 693.

(12) Vicente, M. G. H.; Smith, K. M. *J. Org. Chem*. **1991**, *56*, 4407.

(13) (a) Osuka, A.; Liu, B.-L.; Maruyama, K. *Chem. Lett*. **1993**, 949. (b) Burrell, A. K.; Officer, D.; Reid, D. *Angew. Chem., Int. Ed. Engl*. **1995**, *34*, 900. (c) Osuka, A.; Maruyama, K.; Yamazaki, I.; Tamai, N. *Chem. Phys. Lett.* **1990**, *165*, 392. (d) Osuka, A.; Maruyama, K.; Mataga, N.; Asahi, T.; Yamazaki, I.; Tamai, N. *J. Am. Chem. Soc*. **1990**, *112*, 4958. (e) Yang, S. I.; Lammi, R. K.; Seth, J.; Riggs, J. A.; Arai, T.; Kim, D.; Bocian, D. F.; Holten, D.; Lindsey, J. S. *J. Phys. Chem. B* **1998**, *102*, 9426.

(14) Yoshida, N.; Shimidzu, H.; Osuka, A. *Chem. Lett*. **1998**, 55.

(15) Aratani, N.; Osuka, A.; Kim, Y. H.; Jeong, D. H.; Kim, D. *Angew. Chem., Int. Ed. Engl.* **2000**, *39*, 1458.

(16) Kim, Y. H.; Jeong, D. H.; Kim, D.; Jeoung, S. C.; Cho, H. S.; Kim, S. K.; Aratani, N.; Osuka, A. *J. Am. Chem. Soc*. **2001**, *123*, 76.

(17) (a) Burke, J. M.; Kincaid, J. R.; Spiro, T. G. *J. Am. Chem. Soc.* **1978**, *100*, 6077. (b) Schick, G. A.; Bocian, D. F. *J. Am. Chem. Soc.* **1980**, *102*, 7982. (c) Schick, G. A.; Bocian, D. F. *J. Am. Chem. Soc.* **1983**, *105*, 1830.

(18) Tait, C. D.; Garner, J. M.; Collman, J. P.; Sattelberger, A. P.; Woodruff, W. H. *J. Am. Chem. Soc*. **1989**, *111*, 9072.

(19) Fulton, R. L.; Gouterman, M. *J. Chem. Phys*. **1961**, *35*, 1059.

(20) Adar, F.; Srivastada, T. S.; *Proc. Natl. Acad. Sci. U.S.A.* **1975**, *72*, 4419.

(21) Hwang, Y. N.; Park, S. H.; Kim, D. *Phys. Rev. B* **1999**, *59*, 299.

(22) (a) McRae, E. G.; Kasha, M. *J. Chem. Phys*. **1958**, *28*, 721. (b) Kasha, M. *Radiat. Res*. **1963**, *20*, 55. (c) McRae, E. G.; Kasha, M. In *Physical Process in Radiation Biology*; Academic Press: New York, 1964; p 23. (d) Kasha, M.; Rawls, H. R.; El-Bayoumi, M. A. *Pure Appl. Chem*. **1965**, *11*, 371.

(23) (a) Anderson, H. L. *Inorg. Chem*. **1994**, *33*, 972. (b) O'Keefe, G. E.; Denton, G. J.; Harvey, E. J.; Phillips, R. T.; Friend, R. H. *J. Chem. Phys.* **1996**, *104*, 805.

(24) Kumble, R.; Palese, S.; Lin, V. S.-Y.; Therien, M. J.; Hochstrasser, R. M. *J. Am. Chem. Soc.* **1998**, *120*, 11489.

(25) Yoshida, N.; Osuka, A. Manuscript in preparation.

(26) (a) Reed, R. A.; Purrello, R.; Prendergast, K.; Spiro, T. G. *J. Phys. Chem.* **1991**, *95*, 9720. (b) Atamian, M.; Donohoe, R. J.; Lindsey, J. S.; Bocian, D. F. *J. Phys. Chem.* **1989**, *93*, 2236. (c) Jeoung, S. C.; Kim. D.; Cho, D. W.; Yoon, M. *Bull. Korean Chem. Soc.* **1999**, *20*, 657

(27) (a) Li, X.-Y.; Czernuszewicz, R. S.; Kincaid, J. R.; Su, Y. O.; Spiro, T. G. *J. Phys. Chem.* **1990**, *94*, 31. (b) Rush, T. S., III; Kozlowski, P. M.; Piffat, C. A.; Kumble, R.; Zgierski, M. Z.; Spiro, T. G. *J. Phys. Chem.* **2000**, *104*, 5020.

(28) Snyder, R. G.; Schachtschneider, J. H. *Spectrochim. Acta* **1963**, *19*, 85.

(29) Li, X.-Y.; Czernuszewicz, R. S.; Kincaid, J. R.; Spiro, T. G. *J. Am. Chem. Soc*. **1989**, *111*, 7012, 7024.

(30) Bhuiyan, A. A.; Seth, J.; Yoshida, N.; Osuka, A.; Bocian, D. F. *J. Phys. Chem. B* **2000**, *104*, 10757.

(31) Stein, P.; Ulman, A.; Spiro, T. G. *J. Phys. Chem.* **1984**, *88*, 369.

(32) (a) Albrecht, A. C. *J. Chem. Phys.* **1961**, *34*, 1476. (b) Tang, J.; Albrecht, A. C. In *Raman Spectroscopy Theory and Practice*; Szymanski, H. A., Ed.; Plenum Press: New York, 1970; Vol. 2, pp 33−67. (c) Rousseau, D. L.; Friedman, J. M.; Williams, P. F. In *Topics in Current Physics*; Weber, A., Ed.; Springer: Berlin, 1979; Vol. 11.

(33) Friedman, J. M.; Hochstrasser, R. M. *J. Am. Chem. Soc*. **1976**, *98*, 4043.

(34) Hong, H.; Jacobsen, C. W. *J. Chem. Phys.* **1976**, *65*, 2470.

(35) Berstein, H. J. *Philos. Trans. R. Soc. London, Ser. A* **1979**, *293*, 287.

(36) Clark, R. J. H.; Hester, R. E. *Advances in Infrared and Raman Spectroscopy*; Heyden and Sons: London, 1980; Vol. 6, pp 1−60.

(37) (a) Shelnutt, J. A. *J. Phys. Chem.* **1984**, *88*, 4988, 6121. (b) *J. Phys. Chem.* **1985**, *89*, 4733.

(38) Zerbi, G.; Sandroni, S. *Spectrochim. Acta* **1968**, *24A*, 483.